



Contents lists available at ScienceDirect

Journal of King Saud University – Science

journal homepage: www.sciencedirect.com



Original article

Synthesis of antimicrobial cellulosic derivative and its catalytic activity

Houssni El-Saied^a, Ayman M. Mostafa^{b,*}, Mohamed S. Hasanin^{a,*}, Eman A. Mwafy^c, Asmaa A. Mohammed^d^a Cellulose & Paper Department, National Research Centre, El-Buhouth St., Dokki, Egypt^b Spectroscopy Department, Physics Division, National Research Centre, El-Buhouth St., Dokki, Egypt^c Physical Chemistry Department, Inorganic Chemical Industries and Mineral Resources Division, National Research Centre, El-Buhouth St., Dokki, Egypt^d Medical and Radiation Research Department, Nuclear Materials Authority, Cairo, Egypt

ARTICLE INFO

Article history:

Received 27 April 2018

Accepted 27 June 2018

Available online 3 July 2018

Keywords:

Cellulose acetate

Quercetin

Catalytic degradation

ABSTRACT

Cellulose acetate-quercetin composite was prepared by Solvent exchange technique. The structure and morphology of the prepared samples were analyzed by several spectroscopic tools, Fourier transform Infrared, scanning electron microscope, thermal gravimetric, surface area, zeta potential, and particle sizer. These techniques proved that the prepared composite structure had a decorated needle structure. It had transmittance vibration modes mixing from both precursors. The properties of the composite were changed to be high stability and high mesopore volume than in those precursors. The minimal inhibitory concentration for gram-positive, gram-negative bacteria and fungal strain was studied. The antimicrobial activity of the prepared composites against *Bacillus subtilis* NCID-3610, *Staphylococcus aureus* NCTC-7447, *Pseudomonas aeruginosa* NCID-9016, *E. coli* NCTC-10416 and the unicellular fungi *Candida albicans* NCCLS 11 were recorded to be 0.8, 6.3, 12.5, 6.3 and 0.4 µg/ml, respectively. Also, the reduction-catalytic degradation of harmful 4-Nitrophenol using NaBH₄ in the presence of cellulose acetate-quercetin composite was studied. The time elapsed to complete 28% degradation was found to be 18 min. Thus, these cellulose composites are promising water treatment and preservation materials.

© 2018 The Authors. Production and hosting by Elsevier B.V. on behalf of King Saud University. This is an open access article under the CC BY-NC-ND license (<http://creativecommons.org/licenses/by-nc-nd/4.0/>).

1. Introduction

In the field of environmental protection, hydrocarbons pollutants from industry and autos in the hydrous ecosystem knock the big alarm to the all of the environmental issues (Petrie et al., 2015; Li et al., 2017). Nowadays, the field of water purification from harmful, undesired or hazard elements is very important topic to discuss and study. Nitro group is the one of the unhealthy functional groups that presents in the waste water. These functional groups are used mainly in the daily used materials like textile, food and paper industries (Mittal et al., 2010; Gupta et al., 2011; Ghaedi et al., 2015). In some areas of waste water effluents, the nitro group have concentration reach to 1500 mg L⁻¹ (Khan

et al., 2013) thereby, a lot of attention should be taken to control and overcome on this type of pollutants (Saravanan et al., 2016).

To overcome on like these hazard groups, there are several methods could be used (e.g.: adsorption, ion exchange, and membrane separation) (Saleh and Gupta, 2012; Saravanan et al., 2013a, 2013b; Asfaram et al., 2015; Saravanan et al., 2015a). Amongst these, the catalytic reduction method, one of the most promising methods, has an amazing property as simplicity in the preparation, measurement, and application in a large scale. Moreover, it is a green method has not harmful by-products and produce highly efficient degradation (Zhao et al., 2010; Saravanan et al., 2015b). For that, the reductive-catalytic degradation method can be represented as eco-friendly method with a high efficiency for waste water treatment (Saravanan et al., 2013c; Robati et al., 2016).

Nitrophenols (NP) and their derivatives are the most considerable harmful pollutants in the field of waste water treatment. The United States Environmental Protection Agency warned from nitrophenols and their derivatives as the one of most dangerous pollutants (Saravanan et al., 2013b; Gupta et al., 2014). Keeping in view their toxicity and the possible ways to get rid of them, a lot of studies are concerning on the catalytic reduction of 4-NP to convert it to healthy phenolic compounds.

* Corresponding authors.

E-mail addresses: aymanmdarwish@gmail.com (A.M. Mostafa), sido_sci@yahoo.com (M.S. Hasanin).

Peer review under responsibility of King Saud University.



Production and hosting by Elsevier

<https://doi.org/10.1016/j.jksus.2018.06.007>1018-3647/© 2018 The Authors. Production and hosting by Elsevier B.V. on behalf of King Saud University. This is an open access article under the CC BY-NC-ND license (<http://creativecommons.org/licenses/by-nc-nd/4.0/>).

Numerous methods have been known and used to eliminate 4-NP from liquid waste water, including electrochemical treatment, adsorption, and microbial degradation but these ordinary treatment procedures have some major drawbacks, including limited degradation efficiency, slow degradation rate, high costs and limited conditions, these limitations restrict their application in a large scale (Khan et al. 2017). Consequently, there was a need to find adequate method overcoming all these drawbacks as the catalytic degradation method that depending on the conversion of harmful aromatic nitro compounds to safely aromatic amine compounds by the reduction of 4-NP using borohydride ions (BH_4^-).

One of the awfully considerable polymers and their derivatives is cellulose diacetate (CA) that derived from natural cellulose fibers by the esterification process, and is represents as a new type of the significant carbohydrate polymer, due to its size, morphology, surface chemistry, surface to volume ratio and moderately low cost (Maneerung et al., 2008; Basta et al., 2018). It has been used for water filtration, drug-delivery, production of fibers, membranes, films and plastics, and sensor in the form of nano fibrous membrane (Tungprapa et al., 2007; Goetz et al., 2016). Likewise, Quercetin, (QUC), one of the most common compounds of the natural flavonoids class, has biological and pharmaceutical properties used against several diseases including cancer, cataract, schizophrenia and prostatitis (Mamani-Matsuda et al., 2006). Moreover, It shows antioxidant and antibacterial activities because of its ability to scavenge free radicals and to chelate metal ions (Jurasekova et al., 2012).

In this study, the green composite materials were synthesized from CA and QUC via simple method, followed by discovering the new characteristics of these composites to be applicable at the first time in the catalytic degradation, and to be used as antimicrobial agent. We expected that this study will help to open the route for further development of green composites in the water treatment field. So, herein, the cellulose acetate-quercetin (CA-QUC) composite was synthesized via solvent exchange method, followed by characterization studies. The surface morphology was studied using field emission scanning electron microscopy (FE-SEM). The thermal stability of the prepared composite was investigated by thermo gravimetric and differential analysis (TG-DTA). The changing of the functional groups of the composite structure and the crystallinity calculation were measured using Fourier transform infrared spectroscopy (FT-IR). The surface area of the prepared composite was studied using surface area and pore size analyzer. Then, the particle size distribution and stability of the CA-QUC composite was studied using Zeta-potential and the particle sizer technique. Followed that, the efficiency of reductive-catalytic degradation of 4-NP using the characteristics of CA-QUC composite was tested via UV-Visible spectrophotometer. Also, the anti microbial activity was studied against four bacterial strains, two of them are gram positive and the others are gram negative as well as one fungal strain.

2. Materials and methods

2.1. Materials

Cellulose acetate (CA) purchased from BDH chemicals Ltd. Quercetin (QUC) purchased from Sigma–Aldrich Co. with molecular formula $\text{C}_{15}\text{H}_{10}\text{O}_7$. Sodium borohydride (NaBH_4) was obtained from Sigma–Aldrich Co. 4-Nitrophenol (4-NP) was purchased from LOBA CHEMIE, India.

2.2. Preparation method

2.2.1. Preparation of composite

CA-QUC composite was prepared via solvent exchange method (Tang et al., 2014). The ratio of CA to QUC is 1: 10. Firstly, QUC was

dissolved in DMSO with concentration 10% wt/v which added drop wise to 20% wt/v Cellulose acetate solution in acetone. Then the reaction mixture was started in high speed for one hour at room temperature. Also, the reaction temperature was raised to 100 °C, and let for one hour. The deep greenish yellow color is appeared when the reaction is finished. Then the prepared sample was filtered and dried at 105 °C over night.

2.2.2. Reductive-catalytic study

The reductive-catalytic activities of the CA-QUC composite was investigated by the degradation of 4-NP to 4-aminophenol. In standard quartz cell with a 1 cm path length, 2.77 mL of water was mixed with 25 μL (10^{-2} M) of 4-NP solution and 200 μL of freshly prepared NaBH_4 solution (10^{-1} M). Thereafter, the prepared CA-QUC composite was added to the above mixture. After that, the reduction process was ascertained by recording the UV-visible spectra from 250 nm to 550 nm.

2.2.3. Minimal inhibition concentration (MIC) calculation

Gramm-positive bacteria, and, *Escherichia coli* (NCTC-10416) and *Pseudomonas aeruginosa* (NCID-9016) as Gram-negative bacteria as well as six fungal strains (*Candida albicans* (NCCLS 11) were used. One colony of each microbial strain was suspended in a physiological saline solution (NaCl 0.9% in distilled water at pH 6.5). The initial tested concentration of the composite was 100 $\mu\text{g}/\text{ml}$. The Minimal Inhibitory Concentration (MIC) was calculated as stated previously (Remmal et al., 1993). Different concentrations (100, 50, 25, 12.5, 6.25, 3.125, 1.5625, 0.78125, 0.390625, 0.195313, 0.097656, and 0 as positive control) of the tested substance were prepared through serial dilution method. Mueller Hinton Agar medium was inoculated by the above mentioned bacterial strains and incubated individually at 37 °C for 24 h. After all incubation periods have been elapsed clear zones were measured in mm. The above concentrations were used to determine the MIC value under the same incubation conditions.

2.3. Characterization techniques

A Fourier-transform infrared spectroscopy (FT-IR) was employed to demonstrate the chemical composition of prepared samples by JASCO 6100 spectrometer using KBr method. The morphology and topography of the prepared samples were analyzed by scanning electron microscopy (SEM, Quanta FEG 250, FEI). The particle size distribution and zeta potential of the prepared samples were measured, using Nicomp™ 380 ZLS size analyzer. The thermal degradation was studied using Perkin Elmer thermogravimetric Analyzer TGA7. The Adsorption and desorption of the prepared samples were measured using Surface Area and Pore Size Analyzer NOVA touch LX4, Quantachrome, USA. The catalytic properties of samples were measured in 190–550 nm wavelength range using Agilent Cary 60 spectrophotometer.

3. Results and discussion

3.1. SEM micrographs

Scanning electron microscopy has been employed to investigate the morphology and topography of the surfaces of CA-QUC composite. From Fig. 1, it can be seen that the crystals of QUC are like needle shaped, and CA shaped like a block structure, while the morphology of CA-QUC composite appeared a decorated needle structure proved a successful physical combination between QUC and CA. This combination has a reduction of the crystal size reduced and formed aggregates compared to both intact QUC and

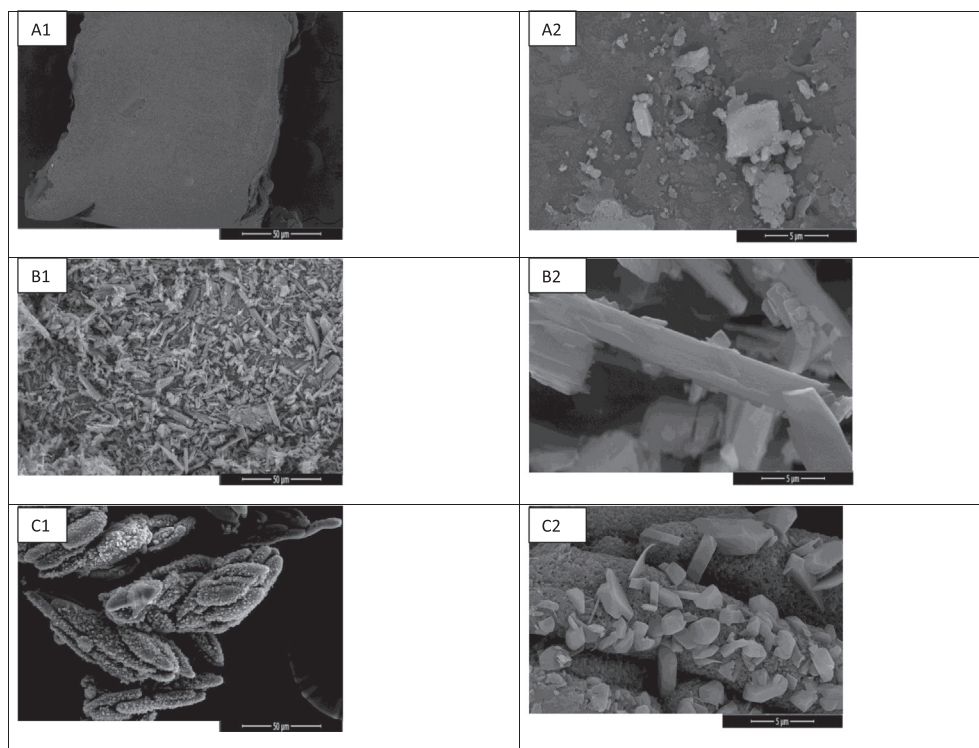


Fig. 1. SEM images of (a) CA, (b) QUC and (c) CA-QUC composite.

CA, manifesting the interaction between QUC and CA (Abou-Kandil et al., 2015; Awad et al., 2015; Zaini et al., 2016).

3.2. FTIR characterization

In Fig. 2, the FT-IR study was used to investigate the functional groups of CA, QUC, and to prove the interaction between CA and QUC.

The characteristics vibrational bands of CA structure were appeared to be as follow: the transmittance broad peak at 3440 cm^{-1} (stretching mode) is due to the presence of hydroxyl group (Darwish et al., 2015). The transmittance bands at 1630 and 1280 cm^{-1} are related to the presence of $\text{C}=\text{O}$ group of esters (stretching mode), and the transmittance bands at 1250 and 1660

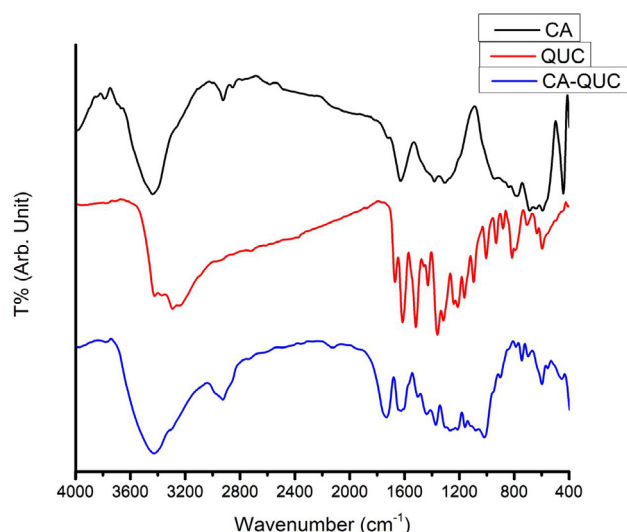


Fig. 2. FT-IR spectra of CA, QUC and CA-QUC composite.

cm^{-1} is corresponding to the presence of $\text{C}=\text{O}$ group of esters (stretching mode) (Mostafa et al., 2017; Rajeswari et al., 2017).

The characteristics vibrational bands of QUC structure were appeared to be as follow: The transmittance peaks at 3430 and 3288 cm^{-1} (stretching mode) due to the presence of hydroxyl group. The transmittance peak at 1370 cm^{-1} was appeared due to OH bending of the phenol group (Darwish et al., 2015). The transmittance peak at 1660 cm^{-1} was appeared corresponding to the presence of $\text{C}=\text{O}$ aryl ketonic structure (stretching mode) (Anis et al., 2018). The transmittance peaks at 1610 and 1515 cm^{-1} was appeared due to the presence of $\text{C}=\text{C}$ aromatic ring (stretching mode). The transmittance peak at 1613 cm^{-1} was appeared due to the presence of in-plane band of $\text{C}-\text{H}$ in aromatic hydrocarbon (bending band). The transmittance peaks at 935 , 814 , 700 , and 595 cm^{-1} was appeared due to the presence of in-plane band of $\text{C}-\text{H}$ in aromatic hydrocarbon (bending band). The transmittance peaks at 1245 , 1200 , and 1164 cm^{-1} was appeared due to the presence of $\text{C}-\text{O}$ functional group in the aryl ether ring (stretching mode), $\text{C}-\text{O}$ functional group in the phenol structure (stretching mode), $\text{C}-\text{CO}-\text{C}$ functional group in the ketone structure (stretching mode), respectively (Catauro et al., 2015; Mwafy et al., 2017).

The characteristics vibrational bands of CA-QUC composite structure were appeared to be as follow: The transmittance peak at 1730 cm^{-1} was appeared due to the presence of $\text{C}=\text{O}$ aryl ketonic structure (stretching mode). The transmittance peaks at 3430 (more broad than peak of QUC) and 3288 cm^{-1} (stretching mode) due to the presence of hydroxyl group. This slight shift, the broadening, and the increase in terms of energy absorption of the OH bending band and the slight broadening of the ketone band suggested that QUC was associated with CA matrix. So, this changes or mixing of transmittance peaks indicating that the interaction are presented between QUC and CA (Mitchell et al., 1957; Skornyakov and Komar, 1998; Catauro et al., 2015).

According to Nelson, O'connor, and Levdiik, the crystallinity index (Cr.I) (Nelson and O'Connor, 1964) and the mean strength

of hydrogen bonds (MHBS) were calculated (Levdik et al., 1967). The FT-IR data was investigated that the Cr.I shows that adding of QUC is improving the composite crystallinity as well as decreasing the composite MHBS which cleared that hydrogen bonds become free and active to carry out the reductive-catalytic degradation. These calculations of crystallinity are appeared in Table 1.

3.3. Thermal analysis

Fig. 3 shows the TGA curves of CA, QUC, and CA-QUC composites. TGA curve was carried out to confirm the thermal stability of the precursor and the resulted composite (Awad et al., 2015; Abou-Kandil et al., 2015, Mwafy et al., 2015). In this figure, it has

Table 1
IR calculations.

| Sample | crystal index, [Abs. (1430 cm ⁻¹)/Abs. (900 cm ⁻¹)] | Main hydrogen bond strength (MHBS), [Abs. (3400 cm ⁻¹)/Abs. (2920 cm ⁻¹)] |
|--------|---|---|
| CA | 1.51226 | 4.176456 |
| QUC | 7.537031 | 1.820391 |
| CA-QUC | 1.980733 | 1.959764 |

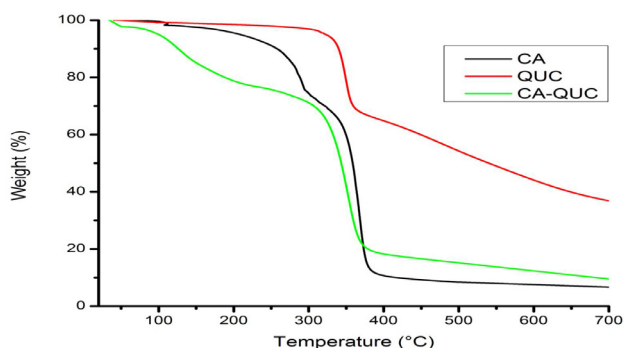


Fig. 3. TGA spectra of CA, QUC and CA-QUC composite.

Table 2
Weight loss (%) of the started reactants and the final composites.

| Samples | Evaporation | | Main decomposition | | | | Residual content wt. (%) | |
|---------|-------------|------------|---------------------|--------|----------------------|-------|--------------------------|-----------------|
| | wt. (%) | Temp. (°C) | Decomposition temp. | | Remaining weight (%) | | | Weight loss (%) |
| | | | T ₀ (°C) | T (°C) | wt. ₀ | wt. | | |
| CA | 96.7 | 109 | 229 | 284.03 | 97.7 | 93.32 | 74.4 | 8.389 |
| QUC | 98.6 | 111.6 | 270 | 324 | 97.7 | 95.58 | 74 | 36.54 |
| CA-QUC | 96.8 | 110 | 288 | 312 | 73.62 | 71.11 | 63.4 | 16.54 |

been shown that about 30 wt% of CA was loosed at around 380 °C. On the other hand, The QUC has two stages to be decomposed; about 20 wt% and 90% of QUC mass loss occurred at around 300 °C and 380 °C, respectively. Also, 80 wt% of CA-QUC composite was loosed around 380 °C (Darwish et al., 2016). From this figure, the CA-QUC composite appeared new thermal characters other than the two starting materials CA and QUC as shown in Table 2. The thermal stability of composite was lower than CA and QUC, respectively. The biodegradable material characterized with lower thermal stability than of that origin (Saravanan et al., 2013c).

3.4. Particle size and zeta potential measurements

From Fig. 4a, the particle size distribution of the CA-QUC composite showed a new band between 100–200 nm, while this band didn't subsist in the two starting samples, this band related to the composite. From Fig. 4b, the zeta potential value and charts cleared that the composite showed high stability in comparison with the two starting materials, all cycles were close to the same value approximately to 7.915mv. In opposite to the two starting materials CA, and QUC displayed unstable chart as shown in Fig. 4b. CA started with approximately 2.4 in the first cycle and ended with 5.38 mv as well as QUC started with approximately with -58 mv and the last cycle was recorded at 4.75 mv this emphasized that the QUC was unstable in its solution.

3.5. Surface area (BET)

Fig. 5 exhibited N₂ adsorption–desorption isotherms at 77 K for the CA, QUC, and CA-QUC composite prepared by solvent exchange method. These isotherms were found to be of type III according to IUPAC classification (Thommes et al., 2015), that they are characteristic of the formation of multilayer followed by pore condensation (a phenomenon whereby a gas condenses to a liquid-like phase in a pore at a pressure (p) less than the saturation pressure (p₀) of the bulk liquid).

From another view, the mesopore volume of the former CA-QUC composite is always higher than that of the precursor of CA or QUC. At a relative pressure where p/p₀ > 0.1, the slope of the isotherm

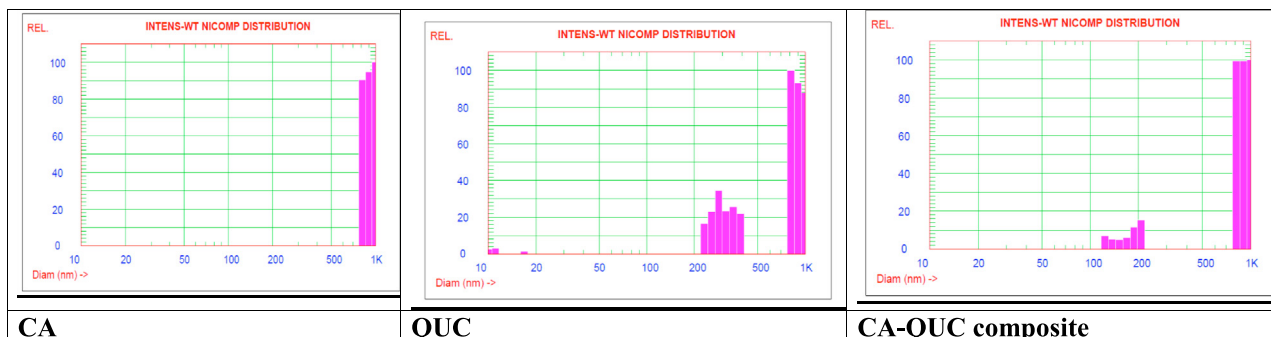


Fig. 4a. Particle sizer of CA, QUC and CA- QUC composite.

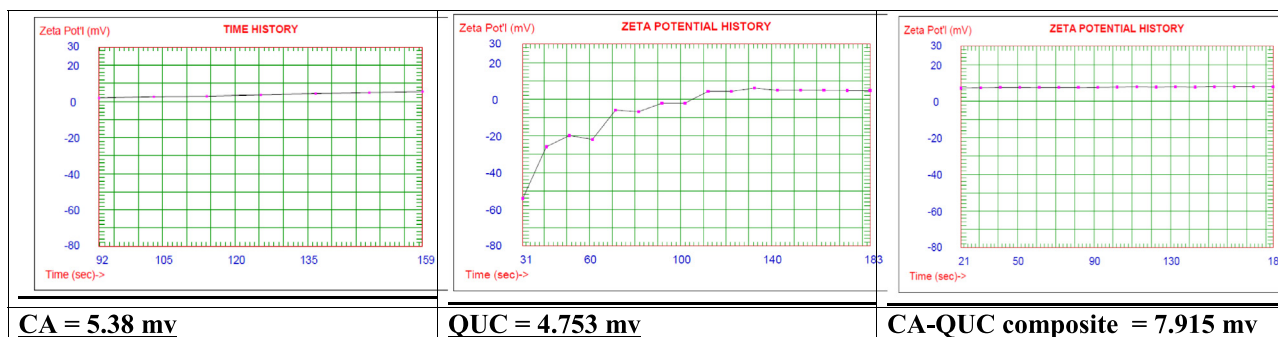


Fig. 4b. Zeta potential of CA, QUC and CA- QUC composite.

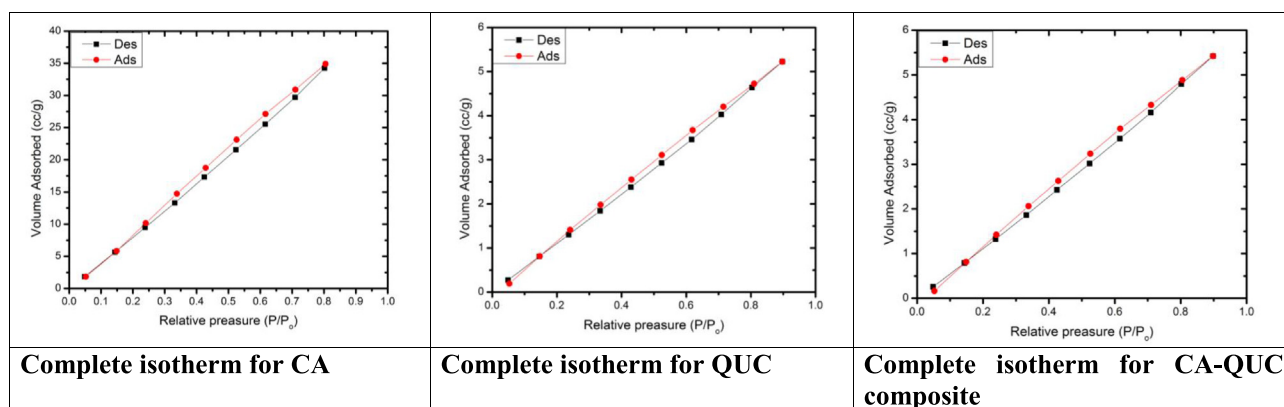


Fig. 5. N₂ adsorption (black line)–desorption (red line) isotherm and BET surface area of CA, QUC and CA-QUC composite. (For interpretation of the references to colour in this figure legend, the reader is referred to the web version of this article.)

plateaus of CA-QUC composite is higher than that of the two starting materials. Concerning CA-QUC composite, the amount of N₂ adsorbed at $p/p_0 = 0.99$ was always higher than that of CA and QUC. The pore texture parameters were calculated as presented in Table 2. It was clearly that CA-QUC composite was the one that manifested the highest BET surface area (S_{BET}) ranging from 3.58 to 26.53 m²/g. By contrast, the total pore volume (TPV) was reduced in CA-QUC composite than that of CA. This takes place according to the increase in the mesopore than macropore and presence of multilayer. This emphasized from the pore radius which increased from 4.59 in CA to 4.73 nm in CA-QUC composite. The S_{meso} and V_{meso} were increased in the composite than CA. This proved that the mesopore of the composite material was higher than the starting materials.

3.6. MIC calculation

The antimicrobial activity of CA-QUC composite was tested against four bacterial strains two of them are gram positive and the others are gram negative as well as one fungal strain. MIC (Minimal Inhibitory Concentration) was measured via plate diffusion method. Considering the composite as anti-bacterial activity, Table 3 and Fig. 6 showed that the composite represent a very strong inhibition affect on the gram positive bacteria, where the

antimicrobial activity against gram positive recorded MIC 0.78125 µg/ml for (*Bacillus subtilis* NCID-3610) and 6.25 µg/ml for *Staphylococcus aureus* NCTC-7447 and these values are desirable values. On another hand, the anti-gram negative (*Escherichia coli* NCTC-10416) performed MIC value of 12.5 µg/ml as well as for *Pseudomonas aeruginosa* NCID-9016 was 6.25 µg/ml and these values are roughly closed to literature values (Basta et al., 2016). The unicellular fungi example is *Candida albicans* NCCLS 11 with MIC value of 0.390625 µg/ml which is the desirable value as anti-fungal agent (Dang et al., 2013). The dual effect of composite is playing an important role in water treatment and preservation (Table 4).

3.7. Catalytic studies

CA-QUC composite structure has revealed superior catalytic performance compared to simple CA structure, thus it can be used to catalyze a number of organic transformations.

In Fig. 7a, an aqueous solution of 4-NP showed two absorption peaks in the UV-Visible spectrum at 319 nm and 403 nm, these peaks are related to 4-NP and tiny amount of 4-nitrophenolate ions, respectively and this absorption spectrum was changed after addition of NaBH₄ as a reducing agent (Dou and Zhang, 2016).

Table 3
BET calculations.

| Sample | S_{BET} , m ² /g | $V_{T(0.95)}$, cm ³ /g | S_{mic} , m ² /g | $S_{mes(BJH)}$, m ² /g | V_{mes} , cm ³ /g | Total Pore Volume, cm ³ /g | Pore radius, nm |
|--------|-------------------------------|------------------------------------|-------------------------------|------------------------------------|--------------------------------|---------------------------------------|-----------------|
| CA | 25.2 | 5.79 | 6.58 | 31.78 | 0.048 | 5.79 | 4.59 |
| QUC | 3.58 | 8.10 | 0.7 | 4.28 | 0.0067 | 8.10 | 4.53 |
| CA-QUC | 26.53 | 4.00 | 5.9 | 32.43 | 0.05 | 6.00 | 4.53 |

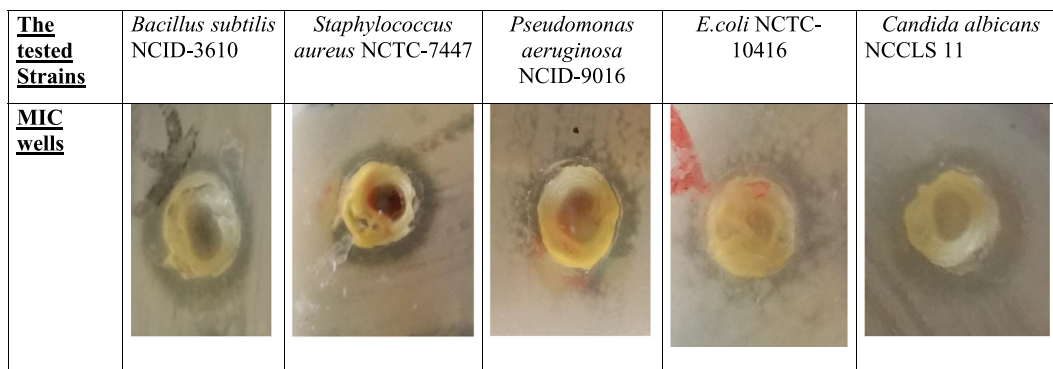


Fig. 6. MIC wells of CA-QUC composite on the tested bacteria and the inhibition zone.

Table 4

MIC ($\mu\text{g/ml}$) of conjugated compound on the tested bacteria and inhibition zone diameters (mm).

| $\mu\text{g/ml}$ | Clear zone/mm | | | | |
|------------------|---------------------------------|-------------------------------|-----------------------------------|------------------------------|--------------------------------|
| | <i>B. subtilis</i> NCID-3610 | <i>S. aureus</i> NCTC-7447 | <i>P. aeruginosa</i> NCID-9016 | <i>E. coli</i> NCTC-10416 | <i>C. albicans</i> NCCLS 11 |
| 100 | 20 | 14 | 7 | 14 | 23 |
| 50 | 19 | 11 | 5 | 13 | 19 |
| 25 | 15 | 8 | 4 | 9 | 17 |
| 12.5 | 9 | 6 | 2 | 5 | 15 |
| 6.25 | 6 | 4 | 0 | 0 | 13 |
| 3.125 | 5 | 0 | 0 | 0 | 11 |
| 1.5625 | 4 | 0 | 0 | 0 | 8 |
| 0.78125 | 2 | 0 | 0 | 0 | 5 |
| 0.390625 | 0 | 0 | 0 | 0 | 3 |
| 0.195313 | 0 | 0 | 0 | 0 | 0 |
| 0.097656 | 0 | 0 | 0 | 0 | 0 |
| 0 | 0 | 0 | 0 | 0 | 0 |

As shown in Fig. 7b, once the catalytic reaction starts, the active hydrogen species are firstly transferred to the surface of NPs by borohydride, then the reduction of 4-NP takes place by the

adsorbed 4-NP molecules and hydrogen ions on the surface. At this time, the intensity value of the absorption peak at 403 nm was decreased gradually and simultaneously the intensity of a new peak at 300 nm was increased and this is related to the reduction of 4-NP to 4-AP. Moreover, it was obviously noticed that 4-NP was converted to 4-AP in a period of about 18 min in the presence of the prepared CA-QUC composite.

Likewise, from the absorbance data in Fig. 7c, when $\ln(A/A_0)$ was plotted versus the reaction time (t), where A_0 and A are the initial and concentration of the 4-nitrophenolate ions and the concentration at time t, respectively, the linear correlation between “ $-\ln(A/A_0)$ ” and the reaction time (t)” showed that this reaction could be represented as pseudo 1st order. For that, the kinetic equation of this reductive-catalytic reaction can be performed as “ $dA/dt = -K_{app} A$ ”. Where k_{app} is the pseudo 1st order rate constant and was determined from the slope of the linear correlation of Fig. 7c (0.0164 min^{-1}) (Mohammadi et al., 2011). The degradation percentage could be calculated by the formula: degradation % = $(1 - \text{final concentration}/\text{initial concentration}) \times 100$. From this formula, (as shown in Fig. 7d) the degradation percentage of the used catalyst was calculated to be nearly 28% in 18 min.

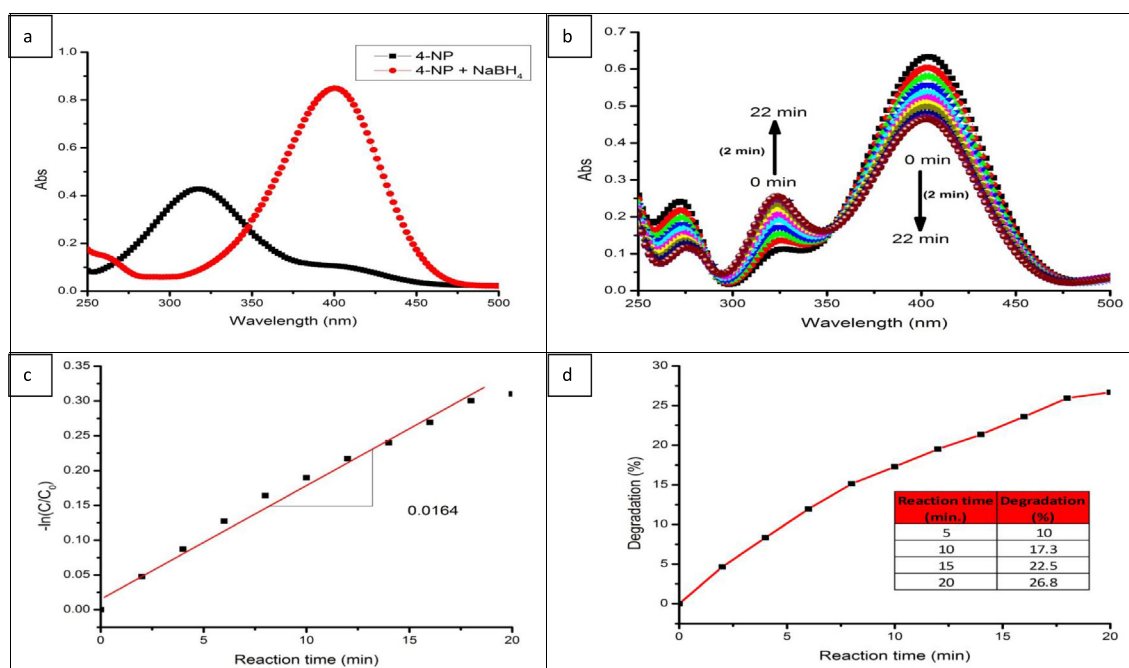


Fig. 7. a) UV-visible absorption spectra of 4-NP before and after addition of NaBH_4 , b) UV-visible spectra changes during the reduction of 4-NP with NaBH_4 over CA-QUC composite, c) $\ln(C/C_0)$ function of reaction time for the reduction of 4-NP over CA-QUC composite, and d) Plot of degradation percentage of reductive rate for the reduction of 4-NP for 22 min.

| Reaction time (min.) | Degradation (%) |
|----------------------|-----------------|
| 5 | 10 |
| 10 | 17.3 |
| 15 | 22.5 |
| 20 | 26.8 |

4. Conclusion

CA-QUC composite was successfully generated from the combination of CA and QUC via solvent exchange method with new characteristic properties of high efficiency as antimicrobial and enhanced reductive-catalytic property. The prepared composite has high stability, complete isotherm with type III, strong inhibition effect on the gram positive bacteria and acceptable thermal stability behavior comparing with the two starting materials

Acknowledgments

The authors express their sincere thanks to National Research Centre of Egypt for providing the necessary research facilities.

References

- Abou-Kandil, A.I. et al., 2015. Polymer nanocomposites part 2: optimization of zinc oxide/high-density polyethylene nanocomposite for ultraviolet radiation shielding. *J. Thermoplast. Compos. Mater.* 28 (11), 1583–1598.
- Anis, B. et al., 2018. Preparation of highly conductive, transparent, and flexible graphene/silver nanowires substrates using non-thermal laser photoreduction. *Optics Laser Technol.* 103, 367–372.
- Asfaram, A. et al., 2015. Removal of basic dye Auramine-O by ZnS: Cu nanoparticles loaded on activated carbon: optimization of parameters using response surface methodology with central composite design. *RSC Adv.* 5 (24), 18438–18450.
- Awad, A. et al., 2015. Polymer nanocomposites part 1: structural characterization of zinc oxide nanoparticles synthesized via novel calcination method. *J. Thermoplast. Compos. Mater.* 28 (9), 1343–1358.
- Basta, A.H. et al., 2016. Properties of modified carboxymethyl cellulose and its use as bioactive compound. *Carbohydr. Polym.* 153, 641–651.
- Basta, A.H. et al., 2018. Green carboxymethyl cellulose-silver complex versus cellulose origins in biological activity applications. *Int. J. Biol. Macromol.* 107, 1364–1372.
- Catauro, M. et al., 2015. Silica/quercetin sol-gel hybrids as antioxidant dental implant materials. *Sci. Technol. Adv. Mater.* 16, (3) 035001.
- Dang, N.T. et al., 2013. Development of intra-vaginal matrices from polycaprolactone for sustained release of antimicrobial agents. *J. Biomater. Appl.* 28 (1), 74–83.
- Darwish, W. et al., 2015. Synthesis and nonlinear optical properties of a novel indium phthalocyanine highly branched polymer. *Polym. Adv. Technol.* 26 (8), 1014–1019.
- Darwish, W.M. et al., 2016. Indium (III) phthalocyanine eka-conjugated polymer as high-performance optical limiter upon nanosecond laser irradiation. *High Perform. Polym.* 28 (6), 651–659.
- Dou, L., Zhang, H., 2016. Facile assembly of nanosheet array-like CuMgAl-layered double hydroxide/rGO nanohybrids for highly efficient reduction of 4-nitrophenol. *J. Mater. Chem. A* 4 (48), 18990–19002.
- Ghaedi, M. et al., 2015. Modeling of competitive ultrasonic assisted removal of the dyes—Methylene blue and Safranin-O using Fe₃O₄ nanoparticles. *Chem. Eng. J.* 268, 28–37.
- Goetz, L.A. et al., 2016. Superhydrophilic anti-fouling electrospun cellulose acetate membranes coated with chitin nanocrystals for water filtration. *J. Membr. Sci.* 510, 238–248.
- Gupta, V.K. et al., 2014. A novel magnetic Fe@ Au core-shell nanoparticles anchored graphene oxide recyclable nanocatalyst for the reduction of nitrophenol compounds. *Water Res.* 48, 210–217.
- Gupta, V.K. et al., 2011. Removal of the hazardous dye—Tartrazine by photodegradation on titanium dioxide surface. *Mater. Sci. Eng., C* 31 (5), 1062–1067.
- Jurasekova, Z. et al., 2012. Adsorption and catalysis of flavonoid quercetin on different plasmonic metal nanoparticles monitored by SERS. *J. Raman Spectrosc.* 43 (12), 1913–1919.
- Khan, F.U. et al., 2017. Novel combination of zero-valent Cu and Ag nanoparticles@ cellulose acetate nanocomposite for the reduction of 4-nitro phenol. *Int. J. Biol. Macromol.* 102, 868–877.
- Khan, R. et al., 2013. Microbial decolorization and degradation of synthetic dyes: a review. *Rev. Environ. Sci. Bio/Technol.* 12 (1), 75–97.
- Levdik, I. et al., 1967. Study of pulp structure by infrared spectroscopy. *Tr. Vses Nauch Issled. Inst. Tsellyul Bum. Prom* 52, 109–111.
- Li, W. et al., 2017. Electrospun H₄ SiW₁₂ O₄₀/cellulose acetate composite nanofibrous membrane for photocatalytic degradation of tetracycline and methyl orange with different mechanism. *Carbohydr. Polym.* 168, 153–162.
- Mamani-Matsuda, M. et al., 2006. Therapeutic and preventive properties of quercetin in experimental arthritis correlate with decreased macrophage inflammatory mediators. *Biochem. Pharmacol.* 72 (10), 1304–1310.
- Maneerung, T. et al., 2008. Impregnation of silver nanoparticles into bacterial cellulose for antimicrobial wound dressing. *Carbohydr. Polym.* 72 (1), 43–51.
- Mitchell, J. et al., 1957. Determination of acetyl content of cellulose acetate by near infrared spectroscopy. *Anal. Chem.* 29 (4), 499–502.
- Mittal, A. et al., 2010. Removal and recovery of Chrysoidine Y from aqueous solutions by waste materials. *J. Colloid Interface Sci.* 344 (2), 497–507.
- Mohammadi, N. et al., 2011. Adsorption process of methyl orange dye onto mesoporous carbon material—kinetic and thermodynamic studies. *J. Colloid Interface Sci.* 362 (2), 457–462.
- Mostafa, A.M. et al., 2017. Au@ CdO core/shell nanoparticles synthesized by pulsed laser ablation in Au precursor solution. *Appl. Phys. A* 123 (12), 774.
- Mwafy, E.A. et al., 2015. High UV-shielding performance of zinc oxide/high-density polyethylene nanocomposites. *Spectrosc. Lett.* 48 (9), 646–652.
- Mwafy, E.A. et al., 2017. Studying the bimetallic catalyst effects on the synthesis of multi-walled carbon nanotubes via CVD method. *Res. J. Pharm. Biol. Chem. Sci.* 8 (1), 375–382.
- Nelson, M.L., O'Connor, R.T., 1964. Relation of certain infrared bands to cellulose crystallinity and crystal lattice type. Part II. A new infrared ratio for estimation of crystallinity in celluloses I and II. *J. Appl. Polym. Sci.* 8 (3), 1325–1341.
- Petrie, B. et al., 2015. A review on emerging contaminants in wastewaters and the environment: current knowledge, understudied areas and recommendations for future monitoring. *Water Res.* 72, 3–27.
- Rajeswari, A. et al., 2017. Preparation, characterization of nano ZnO-blended cellulose acetate-polyurethane membrane for photocatalytic degradation of dyes from water. *Chem. Eng. J.* 313, 928–937.
- Remmal, A. et al., 1993. Improved method for the determination of antimicrobial activity of essential oils in agar medium. *J. Essent. Oil Res.* 5 (2), 179–184.
- Robati, D. et al., 2016. Removal of hazardous dyes—BR 12 and methyl orange using graphene oxide as an adsorbent from aqueous phase. *Chem. Eng. J.* 284, 687–697.
- Saleh, T.A., Gupta, V.K., 2012. Photo-catalyzed degradation of hazardous dye methyl orange by use of a composite catalyst consisting of multi-walled carbon nanotubes and titanium dioxide. *J. Colloid Interface Sci.* 371 (1), 101–106.
- Saravanan, R. et al., 2013a. Visible light induced degradation of methylene blue using CeO₂/V₂O₅ and CeO₂/CuO catalysts. *Mater. Sci. Eng., C* 33 (8), 4725–4731.
- Saravanan, R. et al., 2013b. ZnO/Ag nanocomposite: an efficient catalyst for degradation studies of textile effluents under visible light. *Mater. Sci. Eng., C* 33 (4), 2235–2244.
- Saravanan, R. et al., 2015a. ZnO/Ag/Mn₂O₃ nanocomposite for visible light-induced industrial textile effluent degradation, uric acid and ascorbic acid sensing and antimicrobial activity. *RSC Adv.* 5 (44), 34645–34651.
- Saravanan, R. et al., 2015b. ZnO/Ag/CdO nanocomposite for visible light-induced photocatalytic degradation of industrial textile effluents. *J. Colloid Interface Sci.* 452, 126–133.
- Saravanan, R. et al., 2016. Conducting PANI stimulated ZnO system for visible light photocatalytic degradation of coloured dyes. *J. Mol. Liquids* 221, 1029–1033.
- Saravanan, R. et al., 2013c. The photocatalytic activity of ZnO prepared by simple thermal decomposition method at various temperatures. *J. Mol. Liquids* 177, 394–401.
- Skornyakov, I., Komar, V., 1998. IR spectra and the structure of plasticized cellulose acetate films. *J. Appl. Spectrosc.* 65 (6), 911–918.
- Tang, Z. et al., 2014. A generic solvent exchange method to disperse MoS₂ in organic solvents to ease the solution process. *Chem. Commun.* 50 (30), 3934–3937.
- Thommes, M. et al., 2015. Physisorption of gases, with special reference to the evaluation of surface area and pore size distribution (IUPAC Technical Report). *Pure Appl. Chem.* 87 (9–10), 1051–1069.
- Tungprapa, S. et al., 2007. Release characteristics of four model drugs from drug-loaded electrospun cellulose acetate fiber mats. *Polymer* 48 (17), 5030–5041.
- Zaini, E. et al., 2016. Identification and Characterization of Solid Binary System of Quercetin-Nicotinamide. *Orient. J. Chem.* 32 (3), 1545–1550.
- Zhao, G. et al., 2010. Sorption of heavy metal ions from aqueous solutions: a review. *Open Colloid Sci. J.* 4 (1).